FULL PAPER

Dalton
www.rsc.org/dalton

Doping and defect association in $AZrO_3$ (A = Ca, Ba) and $LaMO_3$ (M = Sc, Ga) perovskite-type ionic conductors †

M. Saiful Islam,* Peter R. Slater, Julian R. Tolchard and Tim Dinges ‡
Materials Chemistry Laboratory, Chemistry Division, University of Surrey, Guildford, UK GU2 7XH. E-mail: m.islam@surrey.ac.uk

Received 20th February 2004, Accepted 5th April 2004
First published as an Advance Article on the web 23rd July 2004

Computer simulation techniques have been used to investigate the defect chemistry of perovskite-structured ionic conductors based upon $AZrO_3$ (A = Ca, Ba) and $LaMO_3$ (M = Sc, Ga). Our studies have examined dopant site-selectivity, oxide ion migration and dopant–defect association at the atomic level. The energetics of dopant incorporation in $AZrO_3$ show strong correlation with ion size. We predict Y^{3+} to be one of the most favourable dopants for $BaZrO_3$ on energetic grounds, which accords with experimental work where this cation is the commonly used acceptor dopant for effective proton conduction. Binding energies for hydroxy–dopant pairs in $BaZrO_3$ are predicted to be favourable with the magnitude of the association increasing along the series Y < Yb < In < Sc. This suggests that proton mobility would be very sensitive to the type of acceptor dopant ion particularly at higher dopant levels. Oxygen vacancy migration in $LaScO_3$ is *via* a curved pathway around the edge of the ScO_6 octahedron. Dopant–vacancy clusters comprised of divalent dopants (Sr, Ca) at the La site have significant binding energies in $LaScO_3$, but very low energies in $LaGaO_3$. This points to greater trapping of the oxygen vacancies in doped $LaScO_3$, perhaps leading to higher activation energies at increasing dopant levels in accord with the available conductivity data.

1 Introduction

Oxygen ion and proton conductivity in perovskite-structured oxides have attracted considerable attention owing to the range of electrochemical applications (*e.g.* fuel cells, gas sensors, ceramic membranes) and the fundamental fascination with transport phenomena in solid state materials. A range of perovskite ceramics, particularly cerates ($ACeO_3$) and zirconates ($AZrO_3$), exhibit significant proton conductivity.[1] An important example is the development of a potentiometric gas sensor for hydrogen in molten metal based upon doped $CaZrO_3$ as the proton-conducting electrolyte.[2] In terms of defect chemistry, the oxide is typically doped by a trivalent cation at the Zr site resulting in the formation of charge-compensating oxygen vacancies, which are readily filled by hydroxy ions in the presence of water vapour.

More recently, there has been renewed interest in acceptor-doped $BaZrO_3$ whose combination of high proton conductivity coupled with good chemical stability,[3–7] makes this material a promising candidate for solid oxide fuel cell (SOFC) applications. Bohn and Schober[5] find that the proton mobility in Y-doped $BaZrO_3$ is among the highest ever reported for a perovskite-type proton conductor. The Y-doped $BaZrO_3$ system has the potential to operate at lower temperatures than the conventional SOFC electrolyte, and hence recent research has involved attempts to optimise the materials' properties. An electrochemical reactor with a ceramic proton-conducting membrane based on doped $BaZrO_3$ has also been used to study the electrochemical promotion of catalysis.[6]

Also in this field of conducting solids, the oxygen transport properties of the $LaGaO_3$-based perovskite have been widely investigated,[8–18] owing to the higher oxygen ion conductivity than the conventional Y/ZrO_2 electrolyte at lower temperatures. The incorporation of cation dopants to form the system $La_{1-x}Sr_xGa_{1-y}Mg_yO_{3-\delta}$ (often termed LSGM) gives rise to the highly mobile oxygen vacancies that are responsible for the observed ionic conductivity. More recently, the oxygen ion and proton conduction properties of the related $LaScO_3$ material have been investigated, particularly systems doped with alkaline-earth dopants at either La or Sc sites.[19–21] For example, Lybye and Bonanos[19] have investigated the $La_{0.9}Sr_{0.1}Sc_{0.9}Mg_{0.1}O_{3-\delta}$ material and showed mixed conductivity at low oxygen partial pressure; proton conduction was dominant at temperatures below 700 °C while above 800 °C oxygen ion conduction became increasingly dominant with temperature. More recently, Kato *et al.*[21] have investigated the electrical conductivity of Al-doped $La_{1-x}Sr_xScO_3$ as a potential SOFC material.

It has become increasingly clear that the investigation of defect phenomena and atomistic diffusion mechanisms underpins the fundamental understanding of macroscopic behaviour. However, there is often limited atomic-scale information on complex ceramic oxides, such as lattice defects, dopant-site selectivity and the extent of defect-dopant clustering. There is also debate as to whether there is any significant interaction between the dopant ion and the protonic defect leading to possible proton "trapping".

This study attempts to provide further insight into these problems by using computer simulation techniques, which are now well established tools in solid state chemistry. The reliability of such an approach has been demonstrated by our simulation studies of defects, ion transport and surface structures of other perovskite oxides (*e.g.* $LaMnO_3$, $LaCoO_3$).[22–25] This paper presents recent computational studies of topical oxygen ion and proton-conducting perovskites based upon $LaScO_3$ and $BaZrO_3$, with direct comparison with related work on $LaGaO_3$ (ref. 23) and $CaZrO_3$ (ref. 22), respectively. Emphasis here is placed on probing dopant site-selectivity, defect association and oxygen ion migration, which have assisted in the further understanding of these complex oxides on the atomic-scale.

2 Computational methods

Our description of the computational techniques will be brief since comprehensive reviews are given elsewhere.[26–29] In this paper, two main classes of technique have been employed in the study of the perovskite materials: atomistic (static lattice) and quantum mechanical (*ab initio*) methods.

† Based on the presentation given at Dalton Discussion No. 7, 5–7th July 2004, University of St Andrews, UK.
‡ Present address: Fachhochschule Gelsenkirchen, D45665 Recklinghausen, Germany.

DOI: 10.1039/b402669c

First, atomistic simulation methods determine the lowest energy configuration of the crystal structure by employing efficient energy minimisation procedures. The calculations rest upon the specification of an interatomic potential model, which expresses the total energy of the system as a function of the nuclear coordinates. For ceramic oxides, the Born model framework is commonly employed which partitions the total energy into long-range Coulombic interactions, and a short-range term to model the repulsions and van der Waals forces between electron charge clouds.[26,27] Because charged defects will polarise other ions in the lattice, electronic polarisibility must be incorporated into the potential model. The shell model provides a simple description of such effects and has proven to be effective in simulating the dielectric and lattice dynamical properties of ceramic oxides. It should be stressed, as argued previously,[26] that employing such a potential model does not necessarily mean that the electron distribution corresponds to a fully ionic system, and that the general validity of the model is assessed primarily by its ability to reproduce observed crystal properties.

An important feature of these calculations is the treatment of lattice relaxation about the point defect, dopant cluster or migrating ion. The Mott–Littleton approach is to partition the crystal lattice into two regions so that ions in a spherical inner region surrounding the defect are relaxed explicitly.[26] In contrast, the remainder of the crystal, where the defect forces are relatively weak, is treated by more approximate quasi-continuum methods. In this way local relaxation is effectively modelled and the crystal is not considered simply as a rigid lattice; these methods are embodied in the GULP simulation code.[27] Energy minimisation methods identify the static configuration of lowest energy and are essentially 'zero Kelvin' calculations. In essence, the empirical interatomic potentials are derived within the context of a room-temperature or higher temperature experimental structure.

Finally, we note that there is an expanding role for quantum mechanical (QM) or *ab initio* methods in solid state studies. The present calculations on proton–dopant binding are performed within the DFT framework, with the exchange–correlation energy being treated using the generalised-gradient approximation of Perdew *et al.*[28] The particular implementation of DFT employed here combines a plane-wave basis set with the total energy pseudo-potential method (as embodied in the CASTEP code[29]) which is ideally suited to calculations on periodic systems. Our simulations are based upon ultrasoft pseudo-potentials with the Brillouin zone sampled according to the Monkhorst–Pack scheme[30] using a 2 × 1 × 2 mesh. The reference atomic valence configurations used to construct the pseudo-potentials are as follows: H ($1s^1$), O ($2s^22p^4$), Ca ($3s^23p^64s^2$) and Zr ($4s^24p^64d^25s^2$). A plane-wave cut-off of 560 eV was selected after monitoring the convergence of the unit cell lattice parameters and atomic coordinates with respect to the number of plane waves. It is worth noting that *ab initio* techniques of this kind have been applied successfully to other oxides including studies of lithium battery materials.[31]

The starting point for the computational work, prior to the investigation of defects and dopants, was the simulation of the equilibrium bulk structures. The perovskite structure is built upon a framework of corner-linked MO_6 octahedra with the A-site ion in a 12-coordinate site. The orthorhombic perovskite structure can exhibit significant tilting of the octahedra from the ideal cubic configuration. The calculated and experimental unit cell parameters for $LaMO_3$ (where M = Ga, Sc) and $AZrO_3$ (where A = Ca, Ba) are listed in Table 1 (using well established potentials that have been derived previously[22–25]). Examination of the values shows good agreement between experimental and simulated structures, with less than 1% deviation in the cell parameters. We also note that the degree of tilting of the octahedra within the orthorhombic structures have been modelled to within 1.5%. This provides a reliable prerequisite for the subsequent defect simulations.

3 Results and discussion

3.1 Dopant site-selectivity and defect association in $AZrO_3$ proton conductors

Incorporation of trivalent dopants into $BaZrO_3$ or $CaZrO_3$ at the Zr^{4+} sites with the corresponding creation of oxygen vacancies is vital to proton dissolution. However, trivalent dopants, such as the lanthanide ion (Ln^{3+}), can be incorporated at either the Zr^{4+} or A^{2+} sites, as depicted in the following defect reactions (using Kröger–Vink notation):

$$\tfrac{1}{2}Ln_2O_3 + Zr_{Zr}^{x} + \tfrac{1}{2}O_O^{x} \rightarrow Ln'_{Zr} + \tfrac{1}{2}V_O^{\bullet\bullet} + ZrO_2 \qquad (1)$$

$$\tfrac{1}{2}Ln_2O_3 + \tfrac{3}{2}A_A^{x} \rightarrow Ln_A^{\bullet} + \tfrac{1}{2}V_A'' + \tfrac{3}{2}AO \qquad (2)$$

In the former case, charge compensating oxygen vacancies ($V^{\bullet\bullet}_O$) are formed, which are readily filled by hydroxy ions ($OH^{\bullet}_O$) in the presence of water vapour, a series of processes that are crucial to proton dissolution:

$$H_2O_{(g)} + V_O^{\bullet\bullet} + O_O^{x} \rightarrow 2OH_O^{\bullet} \qquad (3)$$

Substitution of Ln^{3+} for A^{2+} does not, however, produce the oxygen vacancies that are important for proton uptake as discussed previously.[3,4] Dopant site-selectivity may therefore provide further insight as to why certain dopants do not produce effective proton conductors.

Our simulation approach to dopant substitution involves the calculation of the relative energetics of substitution at both Zr and A sites. The energies of these defect "solution" reactions (eqns. (1) and (2)) can be evaluated by combining appropriate defect and lattice energy terms. In this way, such an approach provides a useful systematic guide to the relative energies for different dopant species at the same site. The interatomic potentials for the dopant ions are those of the corresponding binary metal oxides.[32] We note that A-site vacancy compensation (rather than Zr vacancy compensation) for A-site substitution (eqn. (2)) is considered since it is found to be energetically more favourable in both $BaZrO_3$ and $CaZrO_3$.

The resulting solution energies for a series of trivalent lanthanide ions in cubic $BaZrO_3$ and, for comparison, in orthorhombic $CaZrO_3$ are presented in Fig. 1 as a function of dopant ion size. As an aid to our analysis, we have used the effective dopant ionic radii for six-coordination[33] since 12-coordination values are not available for all the lanthanide ions. In any case, our main concern here is to examine the trend in energetic difference between substitution at A and Zr sites.

Examination of Fig. 1 reveals a degree of correlation with ion size, in which the lowest calculated solution energy infers a preferential substitution. For $CaZrO_3$, smaller trivalent dopants (*e.g.* Sc, Yb) are predicted to substitute preferentially for the Zr ion, while larger lanthanide dopants (*e.g.* Nd, La) substitute for the Ca ion. This can be explained in terms of the "mismatch" in ion size of the dopant ion with Zr^{4+} (r = 0.72 Å) or Ca^{2+} (r = 1.35 Å). The results also show that owing to the larger size of Ba^{2+} (r = 1.60 Å), the majority of lanthanide ions (with the exception of Nd or La) are predicted to substitute preferentially for Zr in $BaZrO_3$, as expected. We predict Y^{3+} to be one of the most favourable dopants for $BaZrO_3$, which accords with experimental work where this cation is the commonly used acceptor dopant for effective proton conduction.

Due to the uncertainty in the precise magnitude of the lattice energies employed, the relative trends are more significant. For

Table 1 Calculated and experimental unit cell parameters of $AZrO_3$ and $LaMO_3$ perovskite oxides

Compound	Unit cell symmetry	Lattice parameter	Calc./Å	Expt./Å
$CaZrO_3$	Orthorhombic	*a*	5.589	5.591
		b	8.055	8.017
		c	5.766	5.761
$BaZrO_3$	Cubic	*a*	4.188	4.199
$LaScO_3$	Orthorhombic	*a*	5.740	5.784
		b	8.014	8.108
		c	5.638	5.688
$LaGaO_3$	Orthorhombic	*a*	5.485	5.527
		b	5.481	5.496
		c	7.752	7.781

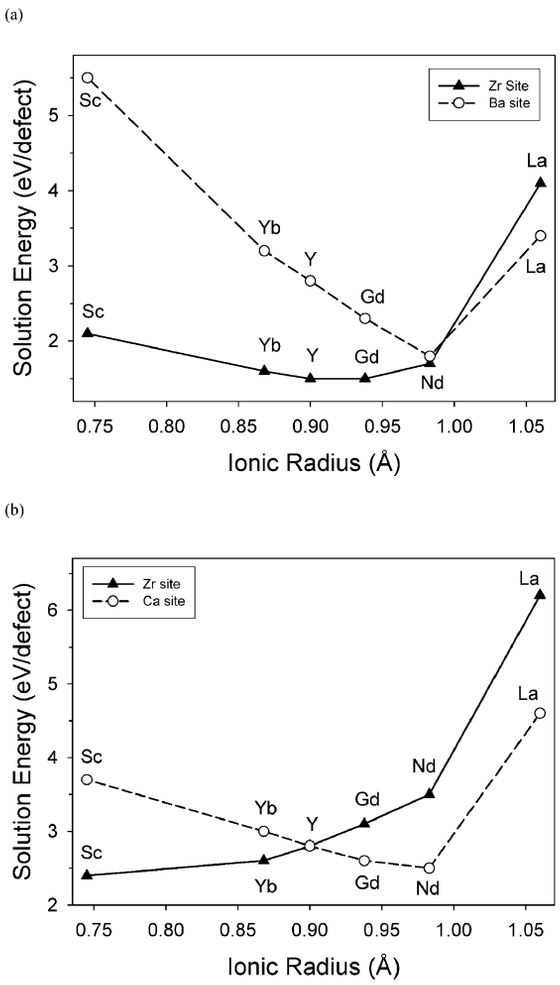

Fig. 1 Calculated energies of solution for trivalent dopants at A and Zr sites *vs.* dopant ion size: (a) $BaZrO_3$ and (b) $CaZrO_3$ (ref. 22). Lines are guide to the eye.

example, it is interesting to note that Y^{3+} in $CaZrO_3$ and Nd^{3+} in $BaZrO_3$ sit at the "crossover" points in Fig. 1, which suggests possible substitution at either A or Zr-sites. Indeed, there is evidence of "amphoteric" dopant ions that can occupy either A or B sites (depending on the A/B ratio) in other perovskite oxides such as $BaTiO_3$.[34] Our simulations also suggest that the lower proton uptake in certain $AZrO_3$ compositions may be partly explained by the preferred substitution of larger dopants (*e.g.* Nd^{3+}) at the A-site; such doping would not create the oxygen vacancies that are required for proton uptake.

In this context, Haile *et al.*[4] find that A-site deficiency in alkaline-earth cerates and zirconates encourages dopant incorporation onto the A-site, rather than the intended M-site, reducing the concentration of oxygen vacancies. Recent studies[4] have proposed that nominally B-site doped $Ba_xCe_{0.85}M_{0.15}O_{3-\delta}$ (x = 0.85–1.20) can exhibit significant Nd dopant partitioning over both Ba and Ce sites.

Table 2 Binding energies of hydroxy–dopant pairs ($OH^{\bullet}_{O}$ M'_{Zr}) at nearest-neighbour sites in $BaZrO_3$

Dopant (M^{3+})	E_{bind}/eV
Sc	−0.74
Y	−0.26
In	−0.58
Yb	−0.35

There has also been debate as to whether there is any significant association between the dopant ion and the protonic defect (hydroxy ion at oxygen site), which may affect proton mobility. In an attempt to probe the question of proton–dopant association, we have extended our previous study[35] on $CaZrO_3$ with a series of calculations on defect pairs ($OH^{\bullet}_{O}$, M'_{Zr}) in $BaZrO_3$ comprised of a hydroxy ion and a neighbouring dopant substitutional (Fig. 2).

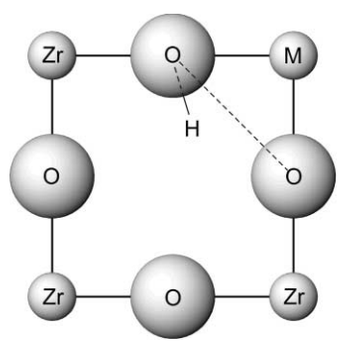

Fig. 2 Schematic representation of a hydroxy–dopant pair at nearest-neighbour sites in $AZrO_3$.

The cluster binding energy (E_{bind}) for this configuration was calculated, which is defined as the difference between the energy of the cluster ($E_{cluster}$) and the sum of the energies of the corresponding isolated defects; this is given by the general relation:

$$E_{bind} = E_{cluster} - \left(\sum_{component} E_{isolated\ defect} \right) \quad (4)$$

where a negative value indicates that the cluster is stable with respect to the component isolated defects. Therefore, in this specific case the binding energy is given by the relation:

$$E_{bind} = E(OH^{\bullet}_{O}\ M'_{Zr}) - \{E(M'_{Zr}) + E(OH^{\bullet}_{O})\} \quad (5)$$

Attention was focused on commonly used dopants in $BaZrO_3$, namely Sc, Y, In, Yb. The resulting energies (reported in Table 2) predict that all the hydroxy–dopant pairs are favourable configurations; the lowest binding energy is for Y and the strongest association is for Sc. These results suggest that proton mobility would be very sensitive to the type of acceptor dopant ion. It may be significant that the lowest predicted binding energy is for Y^{3+}, which is the most commonly used dopant in

the $BaZrO_3$ proton conductor. Kreuer *et al.*[3] have investigated a range of alkaline-earth zirconates and titanates for potential electrochemical applications; they find that the system $BaZr_{1-x}Y_xO_{3-\delta}$ (x = 0.1) exhibits the highest proton mobility and the lowest activation enthalpy. In contrast, the lowest proton mobility and highest activation energy is found for Sc-doped $BaZrO_3$, for which we predict the strongest dopant–OH association.

Although there are no quantitative experimental values for direct comparison, our calculated binding energies are in accord with proton "trapping" energies of about −0.2 and −0.4 eV for related Sc-doped $SrZrO_3$ and Yb-doped $SrCeO_3$ respectively, derived from muon spin relaxation (μSR) and quasi-elastic neutron scattering (QENS) experiments.[36] These studies postulate that in the course of their diffusion, protons are temporarily trapped at single dopant ions.

The present calculations therefore predict possible trapping effects and the presence of proton–dopant pairs particularly in Sc-doped $BaZrO_3$. The different binding energies for the various types of acceptor dopant would be a factor affecting proton mobility. This is analogous to dopant–vacancy association in fluorite-structured oxide ion conductors.[37]

3.2 Mechanism and energetics of oxygen ion migration in $LaMO_3$ perovskites

Our simulation methods have been able to investigate atomic-scale mechanisms of oxygen ion migration in the $LaGaO_3$ and $LaScO_3$ based oxygen ion conductors. The energy profiles for oxygen ion migration were mapped out by calculating the defect energy of the migrating ion along the diffusion path, and allowing relaxation of the lattice ions at each position. It should be noted that interstitial formation and migration are calculated to be highly unfavourable as expected for the perovskite structure.

It is often assumed that the migrating oxide ion takes the shortest path between adjacent anion sites *i.e.*, a direct linear path along the <110> edge of the MO_6 octahedron. Previous empirical approaches have included the geometric concept of the "critical radius" in which oxide ion migration is restricted to a structural gap bordered by two A-site cations and a B-site cation.[38] These investigations assume a hard-sphere model, but do not indicate a non-linear path. Recently, Anderson *et al.*[11] conclude that their conductivity results do not support the critical radius model, and suggest that other factors such as the polarisability of the ions may be important. We stress that our simulation methods include the treatment of polarisability of the ions, and find that local lattice relaxation effects are important when examining oxide ion migration.

Our simulations reveal a small deviation from the direct path for vacancy migration involving a "curved" route around the ScO_6 octahedron edge with the saddle-point away from the adjacent Sc cation, as calculated previously for $LaGaO_3$.[23] Indeed, a neutron scattering study of pure and doped $LaGaO_3$ by Lerch *et al.*[17] provides evidence for our predicted curved path using a detailed analysis of the Debye–Waller factors including anharmonic contributions. More recently, our pathway has also been confirmed by neutron diffraction studies[18] of doped $LaGaO_3$ using the nuclear density distribution. In addition to the $LaScO_3$ and $LaGaO_3$ systems, we have predicted such a curved path for oxygen migration pathway in earlier studies of other perovskite oxides (*e.g.* $LaCoO_3$, $LaYO_3$),[24,25] which hopefully stimulates further experimental work in this area. Although the curved path may not be surprising, we stress that our simulations help to provide a rationalisation based on quantitative calculations on the atomic-scale as opposed to qualitative assumptions.

Oxygen vacancy migration energies can also be derived from the energy profiles; the resulting calculated migration energies for $LaScO_3$ and $LaGaO_3$ are 0.59 and 0.73 eV respectively. It is important to note that these calculated energies (E_m) relate to the intrinsic migration (or jump) of an oxygen vacancy, and do not include energies of defect formation or association. As with fluorite-oxides, the bulk activation energy (E_a) for oxygen ion conduction in perovskites will usually consist of the migration term (E_m) at high temperatures, but an additional binding term (E_{bind}) at low temperatures, leading to two slopes in the conductivity data. This is an issue we discuss further in section 3.3 below.

Table 3 Experimental activation energies for oxygen ion conduction in Sr/Mg doped $LaGaO_3$ for low and high temperature regions

$La_{1-x}Sr_xGa_{1-y}Mg_yO_{3-\delta}$				
x	y	E_a/eV	Temp. range/°C	Ref.
0.10	0.20	0.66	850–1000	9
0.10	0.20	1.13	400–450	9
0.10	0.00	0.81	600–800	10
0.15	0.05	0.92	600–800	10
0.10	0.20	0.73	700–1000	13
0.10	0.20	0.98	450–620	13
0.05	0.05	0.77	595–800	14
0.20	0.05	0.82	595–800	14
0.05	0.20	1.15	595–800	14
0.10	0.20	0.79	550–900	15
0.10	0.00	0.70	800–1000	16

We recognise that direct comparison between our calculated migration energies and the experimental activation energies (E_a) is not straightforward since the E_a values (listed in Table 3) from a range of conductivity studies of doped $LaGaO_3$ show significant variation. This may reflect differences in synthesis conditions, phase purity or analysis of the conductivity data. Nevertheless, the experimental activation energies are generally in the range 0.7–0.8 eV for high temperatures (greater than *ca.* 600 °C), and in the range 0.9–1.1 eV for low temperatures (and high Mg doping levels). The calculated migration energy (0.73 eV) for $LaGaO_3$ is consistent with the experimental activation energies at high temperatures (Table 3). This supports the concept of purely a migration term (E_m) for the oxide ion conductivity data at high temperatures.

For the doped $LaScO_3$ system, it is believed that proton conduction is dominant at temperatures below 700 °C while above 800 °C oxygen ion conduction becomes increasingly dominant with temperature. Lybye *et al.*[19] find that the activation energy for oxygen ion conduction in $La_{0.9}Sr_{0.1}Sc_{0.9}Mg_{0.1}O_{3-\delta}$ is in the range of 0.5 to 1.0 eV. Recent conductivity studies of Kato *et al.*[21] of the $La_{1-x}Sr_xScO_{3-\delta}$ material show that the activation energy increases from 0.63 eV (for x = 0.1) to 1.13 eV (for x = 0.325) within the high temperature region (900–1000 °C).

3.3 Dopant–defect association in $LaMO_3$ perovskites

Interactions between dopant ions and their compensating defects to form distinct clusters is well known in fluorite-structured oxygen ion conductors (*e.g.* doped ZrO_2).[37] Early dielectric relaxation measurements by Nowick *et al.*[39] of acceptor-doped $KTaO_3$ and $CaTiO_3$ perovskites also provide evidence of dopant–vacancy pairs. However, for most perovskite oxides detailed atomic-scale information on defect clusters is limited since experimental determination of such defect structures can be difficult. There has been some debate on dopant–vacancy association in doped $LaMO_3$ perovskites,[12–14,16] but little quantitative data on binding energies. We have therefore carried out, for the first time, a series of calculations on defect pair clusters in doped $LaScO_3$, and compared the results with the much studied $LaGaO_3$ system.

The configurations that were considered are comprised of a dopant substitutional and an oxygen vacancy at nearest-neighbour sites (Fig. 3). The calculated cluster binding energies with respect to the component isolated defects (eqn. (4)) are reported in Table 4 for a range of commonly used divalent

Table 4 Calculated binding energies for {dopant–oxygen vacancy} pair clusters at nearest-neighbour sites in $LaGaO_3$ and $LaScO_3$

		E_{bind}/eV defect^{-1}	
Cation site	Dopant	$LaGaO_3$[a]	$LaScO_3$
A-Site (La)	Ca^{2+}	−0.08	−0.27
	Sr^{2+}	−0.01	−0.22
	Nd^{3+}	−0.07	0.00
B-Site (Ga or Sc)	Mg^{2+}	−0.90	−0.63
	Al^{3+}	−0.30	−0.42
	In^{3+}	−0.45	0.03

[a] Ref. 40 (except for Al).

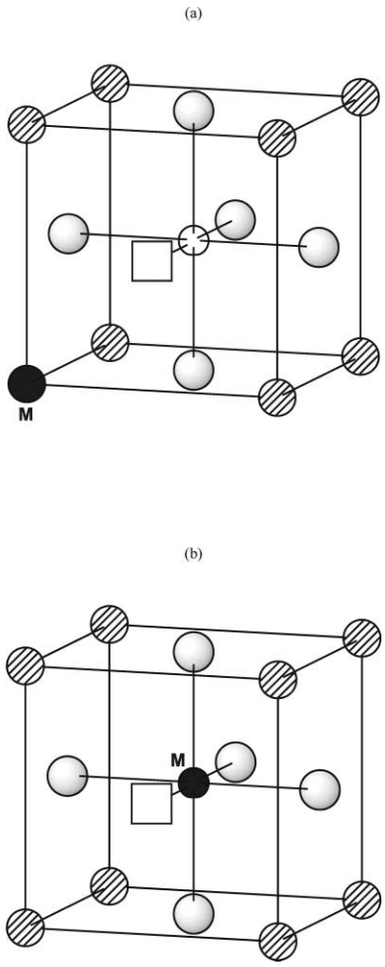

Fig. 3 Dopant (M)–oxygen vacancy (□) pair cluster at nearest-neighbour sites of the $LaScO_3$ or $LaGaO_3$ lattice: (a) dopant ion (M) at La site, (b) dopant ion (M) at Sc or Ga site.

(Mg, Sr, Ca) and trivalent (Al, In, Nd) dopants. Three main points emerge.

First, the clusters with divalent dopants at the La site have very low binding energies in $LaGaO_3$, but significant values of over −0.2 eV in $LaScO_3$. This points to greater trapping of the oxygen vacancies in $LaScO_3$, perhaps leading to lower oxide ion mobility (and a higher activation energy). As noted, recent conductivity studies[21] on the $La_{1-x}Sr_xScO_{3-\delta}$ system show that the activation energy increases from 0.63 eV ($x = 0.1$) to 1.13 eV ($x = 0.325$). In contrast, a zero binding energy is predicted for the Sr-vacancy pair in $LaGaO_3$ suggesting a high "free" vacancy concentration, which would be a major factor in promoting the observed high oxygen ion conductivity in the gallate.

Second, pair clusters involving Mg in both perovskites are found to have strong binding energies, which suggests greater dopant–vacancy association. The results for Mg in the gallate are consistent with the observed increase in the conduction activation energy at higher Mg doping levels in $La_{1-x}Sr_x$-$Ga_{1-y}Mg_yO_{3-\delta}$ (for example, the experimental values from ref. 14 in Table 3). As already noted, this would also lead to two regions or slopes in the conductivity Arrhenius plot: the high temperature region relates to purely the oxygen migration energy (E_m), whereas the low temperature region relates to E_m plus a binding (association) energy term (E_{bind}).

Conductivity studies of the scandate also find a range of activation energies for different doping regimes.[19,20] Lybye *et al.*[19] find that doping only on the La-site (with Sr) seems more effective than "double-doping" with both Sr and Mg. They also speculate that the observed increase in activation energy with decreasing temperature could be due to defect association, as our study clearly predicts. Although Nomura and Tanase[20] mention possible defect association in Sr-doped $LaMO_3$ (where M includes Al, Ga and Sc), they assume that the association enthalpy term is negligible for the Sr dopant. We believe that further experimental work should include binding or association energies within their defect models to rationalise the conductivity data.

Finally, we also examined interactions between trivalent dopants (Al, In, Nd) and oxygen vacancies; these isovalent substitutionals have no "effective" charges (*i.e.* charges relative to the host cation lattice). We note that the oxygen vacancies have already been introduced into the lattice by acceptor dopants. The binding energies (Table 4) indicate a degree of association for some of the trivalent dopants, particularly at the Sc and Ga sites. These results suggest the importance of local "elastic strain" effects in which the binding energy is dependent upon the ion size mis-match between host and isovalent dopant. This is borne out here with the greater ion size mismatch for Al^{3+} (0.53 Å) on the larger Sc^{3+} site (0.74 Å) in the scandate, and In^{3+} (0.80 Å) on the small Ga^{3+} site (0.62 Å) in the gallate.

These strong binding energies suggest that the In^{3+} and Al^{3+} dopants, in particular, would have a detrimental effect on oxygen ion conductivity in which defect association would be a key factor in lowering the free vacancy concentration. This is consistent with findings that show the electrical conductivity in the gallate[12] and scandate[21] decreasing with increasing In and Al concentration respectively. Indeed, Kimpton *et al.*[12] speculate that strong dopant–vacancy association is one of the possible factors for the observed decrease in conductivity with In doping of the gallate material.

The lowest binding energies for the isovalent dopants are calculated for Nd^{3+} at the La site within both perovskites, and In^{3+} at the Sc site in the scandate. These results are analogous to the fluorite-structured oxides in which the minimum in the binding energy occurs when the ionic radius of the host and the dopant are close to each other.[37]

Finally, it is worth noting that we have recently examined[40] the energetics of larger Mg dopant–vacancy "nano-clusters" in the $LaGaO_3$ system based upon ($x\mathrm{Mg}'_{Ga}\ x/2\mathrm{V}_O^{\bullet\bullet}$) with x up to 12. The results suggest that such complex clusters could form at higher dopant concentrations and may be important as precursors to possible short-range ordering or "nano-domain" formation. Current work is extending these simulations to the $LaScO_3$ system and other perovskite oxides.

4 Conclusion

Computer simulation techniques have been used to investigate the defect chemistry of $AZrO_3$ (A = Ca, Ba) and $LaMO_3$ (M = Sc, Ga) perovskite-type ionic conductors, which extends recent modelling work on the calcium zirconate and lanthanum gallate materials. Our studies have attempted to provide a rationalisation of defect properties (such as dopant site-selectivity, oxide ion migration and dopant–defect association) based on quantitative calculations on the atomic-scale as opposed to qualitative arguments. The following main points emerge from our work.

(1) The majority of lanthanide ions (with the exception of Nd and La) are found to substitute preferentially for Zr in $BaZrO_3$ on energetic grounds. We predict Y^{3+} to be one of the most favourable dopants in $BaZrO_3$, which accords with experimental work where this cation is the commonly used acceptor dopant for effective proton conduction. These results also suggest that Nd^{3+} in $BaZrO_3$ and Y^{3+} in $CaZrO_3$ may show "amphoteric" behaviour in which the dopant ion can occupy A and Zr sites.

(2) Binding (or association) energies for hydroxy–dopant pairs in $BaZrO_3$ are predicted to be favourable with the magnitude of the association increasing along the series Y < Yb < In < Sc. This suggests that proton mobility would be very sensitive to the type of acceptor dopant ion. It may be significant that the lowest and highest proton mobilities are observed for Sc- and Y-doped $BaZrO_3$ respectively. Our results are compatible with observed proton "trapping" energies for related perovskites from μSR and QENS experiments.

(3) Oxygen vacancy migration in $LaScO_3$ is *via* a curved path around the edge of the ScO_6 octahedron, which we have simulated previously for other $LaMO_3$ perovskites. There is evidence of our predicted pathway from recent neutron diffraction and neutron scattering studies of the related $LaGaO_3$ system.

(4) Dopant–vacancy clusters comprised of divalent dopants (Sr, Ca) at the La site have significant binding energies in $LaScO_3$, but very low energies in $LaGaO_3$. This points to greater trapping of the oxygen vacancies in doped $LaScO_3$, leading to higher migration activation energies (>1 eV) at low temperatures (and increasing dopant levels), which is consistent with conductivity studies. For the gallate, the negligible binding energy for the Sr dopant–vacancy cluster suggests a high free vacancy concentration, which would be a major factor in promoting the observed high oxide ion conductivity. In contrast, Mg dopant–vacancy clusters have strong binding energies in both the scandate and gallate.

As with fluorite-oxides, the bulk activation energy (E_a) for oxygen ion conduction in doped $LaMO_3$ perovskites will usually consist of the migration term (E_m) at high temperatures, but an additional binding term (E_{bind}) at low temperatures, leading to two slopes in the conductivity data.

(5) Dopant–vacancy association for isovalent (M^{3+}) substitution indicates the importance of elastic strain effects, which depend upon the degree of ion size "mismatch" between host and dopant ion. The strongest binding energy in $LaScO_3$ is found for Al^{3+} on the Sc^{3+}site, which would be detrimental to oxide ion mobility in accord with the available conductivity data.

In general, we believe that further experimental work should include binding (or association) energy terms within the defect models to rationalise the observed conductivity data.

Acknowledgements

We wish to acknowledge the EPSRC, the Computational Chemistry Working Party, and the JREI for Compaq resources at RAL. We are also grateful to Dr R. Andrew Davies for useful discussions.

References

1 K. D. Kreuer, *Solid State Ionics*, 1999, **125**, 285; H. Iwahara, H. Matsumoto and K. Takeuchi, *Solid State Ionics*, 2000, **136–137**, 133; T. Norby, *Solid State Ionics*, 1999, **125**, 1.
2 T. Schober, *Solid State Ionics*, 2003, **162–163**, 277; T. Yajima, K. Koide, H. Takai, N. Fukatsu and H. Iwahara, *Solid State Ionics*, 1995, **79**, 333.
3 K. D. Kreuer, S. Adams, W. Munch, A. Fuchs, U. Klock and J. Maier, *Solid State Ionics*, 2001, **145**, 295; K. D. Kreuer, *Annu. Rev. Mater. Res.*, 2003, **33**, 333.
4 S. M. Haile, G. Staneff and K. H. Ryu, *J. Mater. Sci.*, 2001, **36**, 1149; J. R. Wu, L. P. Li, L. Espinosa and S. M. Haile, *J. Mater. Res.*, 2004, in press.
5 H. G. Bohn and T. Schober., *J. Am. Ceram. Soc.*, 2000, **83**, 768; T. Schneller and T. Schober, *Solid State Ionics*, 2003, **164**, 131.
6 D. Poulidi, M. A. Castillo-del-Rio, R. Salar, A. Thursfield and I. S. Metcalfe, *Solid State Ionics*, 2003, **162**, 305; J. H. Cheng and A. Navrotsky, *J. Mater. Res.*, 2003, **18**, 2501.
7 B. Groß, C. Beck, F. Meyer, T. Krajewski, R. Hempelmann and H. Altgeld, *Solid State Ionics*, 2001, **145**, 325.
8 T. Ishihara, H. Matsuda and Y. Takita, *J. Am. Chem. Soc.*, 1994, **116**, 3801; M. Feng and J. B. Goodenough, *Eur. J. Solid State Inorg. Chem.*, 1994, **31**, 663.
9 J. Drennan, V. Zelizko, D. Hay, F. T. Ciacchi, S. Rajendran and S. P. S. Badwal, *J. Mater. Chem.*, 1997, **7**, 79.
10 P. Huang and A. Petric, *J. Electrochem. Soc.*, 1996, **143**, 1644.
11 P. S. Anderson, G. C. Mather, F. M. B. Marques, D. C. Sinclair and A. R. West., *J. Eur. Ceram. Soc.*, 1999, **19**, 1665.
12 J. Kimpton, T. H. Randle, J. Drennan and G. Auchterlonie, *Mater. Res. Bull.*, 2001, **36**, 639.
13 H. Ullmann, N. Trofimenko, A. Naoumidis and D. Stover., *J. Eur. Ceram. Soc.*, 1999, **19**, 791; L. Vasylechko, V. Vashook, D. Savytskii, A. Senyshyn, R. Niewa, M. Knapp, H. Ullmann, M. Berkowski, A. Matkovskii and U. Bismayer, *J. Solid State Chem*, 2003, **172**, 396.
14 K. Huang, R. S. Tichy and J. B. Goodenough, *J. Am. Ceram. Soc.*, 1998, **81**, 2565; K. Huang, J. Wan and J. B. Goodenough, *J. Mater. Sci.*, 2001, **36**, 1093.
15 T. Ishihara, J. A. Kilner, M. Honda and T. Takita, *J. Am. Chem. Soc.*, 1997, **119**, 2747.
16 V. V. Kharton, A. P. Viskup, A. A. Yaremchenko, R. T. Baker, B. Gharbage, G. C. Mather, F. M. Figueirido, E. N. Naumovich and F. M. B. Marques, *Solid State Ionics*, 2000, **132**, 119.
17 M. Lerch, H. Boysen and T. Hansen, *J. Phys. Chem. Solids*, 2001, **62**, 445.
18 M. Yashima, K. Nomura, H. Kageyama, Y. Miyazaki, N. Chitose and K. Adachi, *Chem. Phys. Lett.*, 2003, **380**, 391.
19 D. Lybye and N. Bonanos, *Solid State Ionics*, 1999, **125**, 339; D. Lybye, F. W. Poulsen and M. Mogensen, *Solid State Ionics*, 2000, **128**, 91; C. Hatchwell, N. Bonanos and M. Mogensen, *Solid State Ionics*, 2003, **162/163**, 93.
20 K. Nomura and S. Tanase, *Solid State Ionics*, 1997, **98**, 229; H. Fujii, Y. Katayama, T. Shimura and H. Iwahara, *J. Electroceram.*, 1998, **2**, 119.
21 H. Kato, T. Kudo, H. Naito and H. Yugami, *Solid State Ionics*, 2003, **159**, 217.
22 R. A. Davies, M. S. Islam and J. D. Gale, *Solid State Ionics*, 1999, **126**, 323.
23 M. S. Islam, *J. Mater. Chem.*, 2000, **10**, 1027; M. S. Khan, M. S. Islam and D. R. Bates, *J. Phys. Chem. B.*, 1998, **102**, 3099.
24 R. A. De Souza, M. S. Islam and E. Ivers-Tiffee, *J. Mater. Chem.*, 1999, **9**, 1621; E. Ruiz-Trejo, M. S. Islam and J. A. Kilner, *Solid State Ionics*, 1999, **123**, 121; M. S. D. Read, M. S. Islam, G. W. Watson, F. King and F. E. Hancock, *J. Mater. Chem.*, 2000, **10**, 2298.
25 M. Cherry, M. S. Islam and C. R. A. Catlow, *J. Solid State Chem.*, 1995, **118**, 125.
26 *Computer Modelling in Inorganic Crystallography*, ed. C. R. A. Catlow, Academic Press, San Diego, CA, 1997.
27 J. D. Gale and A. L. Rohl, *Mol. Simul.*, 2003, **29**, 291.
28 J. P. Perdew, K. Burke and Y. Wang, *Phys. Rev. B*, 1996, **54**, 16533.
29 M. C. Payne, M. P. Teter, D. C. Allan, T. A. Arias and J. D. Joannopoulos., *Rev. Mod. Phys.*, 1992, **64**, 1045.
30 H. J. Monkhorst and J. D. Pack, *Phys. Rev. B*, 1976, **13**, 5188.
31 M. S. Islam, R. A. Davies and J. D. Gale, *Chem. Mater.*, 2003, **15**, 4280; D. Carlier, A. Van der Ven, C. Delmas and G. Ceder, *Chem. Mater.*, 2003, **15**, 2651.
32 G. V. Lewis and C. R. A. Catlow, *J. Phys. C.*, 1985, **18**, 1149.
33 R. D. Shannon, *Acta Crystallogr., Sect. A.*, 1976, **32**, 751.
34 Y. Tsur, A. Hitomi, I. Scrymgeour and C. A. Randall, *Jpn. J. Appl. Phys.*, 2001, **40**, 255; J. Zhi, A. Chen, Y. Zhi, P. M. Vilarinho and J. L. Baptista, *J. Am. Ceram. Soc.*, 1999, **82**, 1345.
35 M. S. Islam, R. A. Davies and J. D. Gale, *Chem. Mater.*, 2001, **13**, 2049.
36 R. Hempelmann, M. Soetratmo, O. Hartmann and R. Wappling, *Solid State Ionics*, 1998, **107**, 269; C. Karmonik and R. Hempelmann, *Phase Transitions*, 1996, **58**, 175.
37 J. A. Kilner, *Solid State Ionics*, 2000, **129**, 13; J. W. Fergus, *J. Mater. Sci.*, 2003, **38**, 4259; C. R. A. Catlow, *Solid State Ionics*, 1984, **12**, 67.
38 J. A. Kilner and R. J. Brook, *Solid State Ionics*, 1982, **6**, 237; J. Ranlov, N. Bonanos, F. W. Poulsen and M. Mogenson, *Solid State Phenom.*, 1994, **39–40**, 219.
39 A. S. Nowick, S. Q. Fu, W. K. Lee, B. S. Lim and T. Scherban, *Mater. Sci. Eng. B.*, 1994, **23**, 19.
40 M. S. Islam and R. A. Davies, *J. Mater. Chem.*, 2004, **14**, 86.